Available online at www.sciencedirect.com
SCIENCE DIRECT®
Journal of Nuclear Materials 324 (2004) 52–61
journal of nuclear materials
www.elsevier.com/locate/jnucmat

Development of a fundamental crack tip strain rate equation and its application to quantitative prediction of stress corrosion cracking of stainless steels in high temperature oxygenated water

Q.J. Peng *, J. Kwon, T. Shoji

Fracture Research Institute, Graduate School of Engineering, Tohoku University, Aoba 01, Aramaki, Aoba-ku, Sendai City 980-8579, Japan

Received 3 February 2003; accepted 13 September 2003

Abstract

A formulation for the quantitative calculation of the stress corrosion cracking (SCC) growth rate was proposed based on a fundamental-based crack tip strain rate (CTSR) equation that was derived from the time-based mathematical derivation of a continuum mechanics equation. The CTSR equation includes an uncertain parameter r_0, the characteristic distance away from a growing crack tip, at which a representative strain rate should be defined. In this research, slow strain rate tensile tests on sensitized 304L stainless steel in oxygenated high temperature water were performed. By curve fitting the experimental results to the numerically calculated crack growth rate, the parameter r_0 was determined. Then, the theoretical formulation was used to predict the SCC growth rates. The results indicate that r_0 is on the order of several micrometers, and that the application of the theoretical equation in predicting the crack growth rate provides satisfactory agreement with the available data.

PACS: 28.41.Qb; 81.40.Np; 81.70.Bt; 46.30.Nz; 2.20.Mk

1. Introduction

Stress corrosion cracking (SCC) of structural components is one major concern in energy and related aqueous systems. Such cracking can affect the reliability, integrity and economics of power plants, and may become a potential service life limiting issue. Indeed, many stainless steel (SS) internal components are subject to intergranular stress corrosion cracking (IGSCC) in boiling water reactor (BWR) operating environments [1]. Efforts have been made to understand the underlying mechanism of SCC and to develop predictive models for lifetime estimation. While significant progress has been made in establishing SCC test procedures, the methodology for the application of laboratory test data to in-plant conditions, such as loading and environmental ones, is less well defined. The main problems associated with extrapolation lie in the time dependence of SCC and the multiplicity of interacting variables – applied stress, material, and environment [2].

Of all the mechanisms associated with SCC, the slip/dissolution–oxidation model has been accepted by many researchers as a reasonable description of SCC in an oxygenated aqueous system [3–5]. The rate-controlling factors to determine the crack growth rate (CGR) in this model are the rupture rate of the oxide film, the rate of repassivation (the reformation of the oxide film), and the

* Corresponding author. Tel.: +81-22 217 7520; fax: +81-22 217 7543.
E-mail address: peng@rift.mech.tohoku.ac.jp (Q.J. Peng).

0022-3115/$ - see front matter © 2003 Elsevier B.V. All rights reserved.
doi:10.1016/j.jnucmat.2003.09.008

rate of diffusion of dissolved metal ions away from the crack tip. Assuming that the oxidation current density decay may occur according to a power law in crack tip alloy environment systems, the average CGR is given by [5]:

$$\dot{a} = \frac{M}{z\rho F} \times \frac{i_0(t_0)^m}{(1-m)(\varepsilon_f)^m} \times (\dot{\varepsilon}_{ct})^m, \quad (1)$$

where $\dot{a}$ is the CGR, M and ρ are the atomic weight and density of the metal respectively, F the Faraday's constant (96 500 Coulomb/equivalent), z the number of electrons involved in the overall oxidation of the metal atom, i_0 the oxidation current density (initial metal dissolution rate) on the bare surface of the crack tip, t_0 the duration of constant current density i_0, ε_f the strain to fracture of the oxide film, m the slope of the current decay curve (the repassivation rate) and $\dot{\varepsilon}_{ct}$ the crack tip strain rate, which embodies the mechanical contributions.

A critical requirement for the application of this model, as can be seen in the above equation, is to define parameters relevant to the mechanics and the environment of the crack tip. These are the crack tip strain rate and parameters related to the repassivation kinetics.

The crack tip strain rate (CTSR) determines the periodicity at which slip-induced film rupture occurs and thus is fundamentally important, unlike the classical design parameters of residual and applied stress, stress intensity, loading frequency etc. [6]. The contribution of CTSR to SCC has been widely recognized and Eq. (1) is valid for CGR prediction of most growing SCC cracks [6–13].

Analysis of data and modeling experiments show that the crack tip strain rate is not a measurable parameter [6,14]. The strain of interest is very local to the crack tip region, where the stress is very high. A fundamentally-based CTSR equation is always required for SCC life prediction, and this has been the most theoretically challenging parameter to quantitative evaluation of CGR. Many attempts have been made to quantify the CTSR using numerical and analytical methods. The following part reviews such methodology developments.

1.1. Semiempirical formulation of CTSR

Semiempirical evaluations of the relationships between CTSR and engineering parameters were made by Ford et al. [6,7], especially, for stainless steel at 288 °C under constant load and moderate stress intensity factors, the CTSR equation is given by

$$\dot{\varepsilon}_{ct} = 4.1 \times 10^{-14} K^4, \quad (2)$$

where $\dot{\varepsilon}_{ct}$ is in the unit of s^{-1} and K, the stress intensity factor, is in the unit of MPa $m^{0.5}$. An examination of the validity of Eq. (2) showed that it could be rationalized in terms of its ability to normalize the effect of a wide range of stressing conditions on the SCC growth rate. Nevertheless, the approach is not based on a fundamental knowledge of the dynamics of crack tip plasticity.

1.2. Approximately evaluation based on crack tip opening displacement rate

Attempts were also made for the quantification of CTSR based on the evaluation of crack tip opening displacement rate. By using finite element methods, Rice et al. [15] proposed a near-tip expression for evaluations of the crack opening displacement rate for a steady growing crack under plain-strain, small-scale yielding conditions in elastic-perfectly plastic solids (no strain-hardening):

$$\dot{\delta} = \alpha \dot{J}/\sigma_y + \beta(\sigma_y/E)\dot{a}\ln(R/x), \quad (3)$$

where $\dot{\delta}$ is the crack tip opening displacement rate, $\dot{J}$ the rate of change in J-integral with time, $\dot{a}$ the crack growth rate, σ_y the yield strength, E the Young's modulus, x the distance from the growing crack tip for evaluation of the crack opening displacement rate, β, α and R are constants.

Eq. (3) can be converted to an approximate expression of the crack tip strain rate by making an appropriate assumption for the length parameter, r, which may be taken to equal the crack tip opening displacement for convenience or the total width of the active flow bands [8–10,16,17]. Therefore, the crack tip strain rate can be given by

$$\dot{\varepsilon}_{ct} = \dot{\delta}/r. \quad (4)$$

Eq. (4) is a useful approach for relative comparison of strain rate effects [12]. However, it does not correlate EAC behavior quantitatively [12]. Furthermore, Eq. (4) can not be applied to work-hardening materials and the selection of a gauge length, r, is arbitrary.

1.3. An equation for fundamental evaluation of CTSR in work-hardening materials

Theoretical strain distributions at a stationary or growing crack tip were studied by using numerical, analytical and experimental approaches. Validities of the theoretical formulations were experimentally examined by measuring the in situ crack tip plastic strain at a pre-existing fatigue crack using stereomicroscopy and electron channeling methods [18–20]. Measurements of a growing fatigue crack in Fe–3wt% Si single crystals indicated that, the plastic crack tip strain equation proposed by Gao and Hwang [21], as shown below, for a growing crack in work hardening materials under plane strain conditions best predicted the strain profile ahead of the crack tip:

$$\varepsilon_p = \beta \frac{\sigma_y}{E}\left[\ln\left(\frac{R_p}{r}\right)\right]^{n/n-1}, \quad (5)$$

where β is a dimensionless constant, σ_y and E are the yield strength and elastic modulus of the material, $R_p = \lambda(K/\sigma_y)^2$ is the plastic zone size, n the strain-hardening exponent in the Ramberg–Osgood power law and r the distance from a growing crack tip.

Eq. (5) was derived on the assumption that a crack grows steadily under quasi-static constant loading. Such an assumption might lead to the limits to the application of Eq. (5). However, the strain distribution for an elastic–plastic growing crack proves to give the best fit to the experimental data to date, albeit it requires corroboration [18].

Suggesting that the analytical strain rate equation should include a term for the rate of change of strain with distance in front of the crack tip, owing to the accumulation of strain as the crack growth, Eq. (5) can be time-derivated. The resultant equation simply implies the rate of change in plastic strain at the crack tip, which corresponds to the crack tip strain rate [22,23]:

$$\dot{\varepsilon}_{ct} = \frac{\beta\sigma_y n}{E(n-1)}\left(2\frac{\dot{K}}{K} + \frac{\dot{a}}{r_0}\right)\left\{\ln\left[\frac{\lambda}{r_0}\left(\frac{K}{\sigma_y}\right)^2\right]\right\}^{1/n-1}, \quad (6)$$

where $\dot{K}$ is the rate of change in K, r_0 the characteristic distance at the crack tip, where the strain rate should be defined. Eq. (6) allows determination of the effects of K, $\dot{a}$, σ_y, $\dot{K}$ and n on CTSR. The analytical solutions to Eq. (6), however, are complicated by the presence of the uncertain variable, r_0. In order to implement the theoretical equation in estimating the CTSR and CGR, the determination of the characteristic distance, r_0 is necessary.

It should be stated here that the possible effect of creep on the crack tip strain rate is not considered in Eq. (6). Creep has been shown to occur in reactor materials at reactor operating temperatures [24,25]. Nevertheless, it can be estimated that the CTSR is strongly dependent on strain redistribution associated with the growing crack for the fast crack growth rate [24]. As for the slow crack growth rate, (e.g. when there is little corrosion at the crack tip for unsensitized materials and/or at low corrosion potentials), the creep behavior may play a larger role in determining the CTSR [24].

Despite the effects of creep on CTSR is not included in Eq. (6) and the possible limitations of Eq. (5), Eq. (6) provides us a fundamental way to quantify crack tip strain rate based on engineering parameters. Validation evaluation of Eq. (6) is highly required [22,23].

1.4. Objectives of the current research

The first objective of this research is to determine the only undetermined parameter, r_0 in Eq. (6). Due to the difficulty in the experimental measurement of CTSR, the method used in this study is the inverse analysis that is based upon the experimental crack growth rate and the theoretical crack growth rate. By incorporating Eq. (6) into Eq. (1), a unique equation for quantitative calculations of CGR is obtained [22], as shown in the following:

$$\dot{a} = \frac{Mi_0}{z\rho F(1-m)}\left(\frac{t_0}{\varepsilon_f}\right)^m \times \left\langle \frac{\beta\sigma_y n}{E(n-1)}\left(2\frac{\dot{K}}{K} + \frac{\dot{a}}{r_0}\right)\left\{\ln\left[\frac{\lambda}{r_0}\left(\frac{K}{\sigma_y}\right)^2\right]\right\}^{\frac{1}{n-1}}\right\rangle^m. \quad (7)$$

In the above equation, all factors affecting the SCC events are taken into account – applied load, material property, and water chemistry. In addition, the general behavior of SCC (stress intensity factor vs. CGR) can be described in terms of Eq. (7), which represents the threshold and plateau behavior in the SCC process [23]. No assumptions, such as diffusion limiting processes nor a critical crack tip solution, are involved.

The experimental CGRs, i.e. the changes in the CGR as a function of loading and time, used for the inverse analysis to optimize the characteristic distance through the numerical calculation, were from slow strain rate tensile (SSRT) tests on sensitized 304L stainless steel in high temperature (288 °C) oxygenated water, simulating the BWR environment. The purpose of finding the characteristic distance is to apply Eqs. (6) and (7) for quantitative calculation of the CTSR and CGR, to evaluate the validity of the equations. This is the second objective of this study. We demonstrated the quantitative validity of the theoretical equations by calculating the CGR under constant load. Predictions for the CGR under simulated BWR conditions are compared with the observed CGR data.

2. SSRT tests on sensitized 304L stainless steel in oxygenated water at 288 °C

2.1. Material and specimen

One-inch thick-compact tension (1T-CT) specimens fabricated from sensitized 304L stainless steel were used for the SSRT tests. Before the tests, all of the specimens were first fatigue-pre-cracked in air at room temperature and then 1.2 mm-deep side grooves were machined. The chemical composition and mechanical properties of the test material are listed in Table 1. The sensitization process was 650 °C × 100 h + air-cooling + 620 °C × 100 h + air-cooling. The resultant electrochemical potentiokinetic reactivation (EPR) value measured by the double-loop method [26] was about 12%.

Table 1
Chemical composition (wt%) and mechanical properties of 304L SS at room temperature

C	Si	Mn	P	S	Cr	Ni	Yield strength	Tensile strength	Elongation
0.012	0.69	1.46	0.005	0.006	18.55	12.08	228 MPa	517 MPa	62%

2.2. Test conditions and procedure

Three SSRT tests with different extension rates were performed. Test conditions are listed in Table 2. All the SSRT tests were conducted in simulated BWR water containing controlled amounts of oxygen. For test 3, in situ pre-cracking was carried out by applying a triangular wave loading at $K_{max} \approx 15$ MPa $m^{0.5}$ and R (load ratio) = 0.2–0.6. The crack growth behavior during the tests was monitored by using an alternating current potential drop (ACPD) technique, which has previously been applied to the monitoring of crack growth tests in high temperature water [27]. The ACPD-based crack length was linearly corrected by the crack length measured on the fracture surface of the specimen. Changes of loading with time during the tests were also monitored. The history of crack propagation and applied load was used to calculate the CGR and stress intensity factor. Changes of the ACPD-based crack length were interpolated with a polynomial equation as a function of time. Then, the CGR was obtained from the time-derivative of the polynomial equation. Changes of K were calculated according to ASTM E399-90 [28] based on the change of load and crack length with time in each test. The fracture surfaces were observed using scanning electron microscopy (SEM) after the SSRT tests to measure the final crack length and investigate the fracture morphology.

2.3. Test results

2.3.1. Initiation and growth of the SCC

The variation of ACPD with time during test 1 and 2 are quite similar. The ACPD-based crack length, as well as the measured ACPD values in test 1 is shown in Fig. 1. The potential rose rapidly in the early stages of the tests, which is commonly observed in the SSRT tests and is believed to be caused by the formation of a local plastic zone at a crack tip without cracking in metals [23]. It is, therefore, assumed that a crack would start to grow at the point of departure from a constant potential, as shown in Fig. 1. Unlike tests 1 and 2, continuously increasing from the beginning of the test rather than the initial rapid increase in ACPD was observed in test 3. This was due to the in situ pre-cracking as stated above. Dependences of the CGR on K for the three SSRT tests are presented in Fig. 2. The CGR and the

Table 2
Test conditions

Parameters	Conditions
Dissolved oxygen	>20 ppm
Flow rate	About one volume exchange per hour
Conductivity (outlet)	0.3–0.4 μS/cm for tests 1 and 2, 0.2–0.4 μS/cm for test 3
Pressure	8.4 MPa
Temperature	288 °C
Extension rate (m/s)	Test 1 5.9×10^{-9}, test 2 1.2×10^{-9}, test 3 7.0×10^{-10}

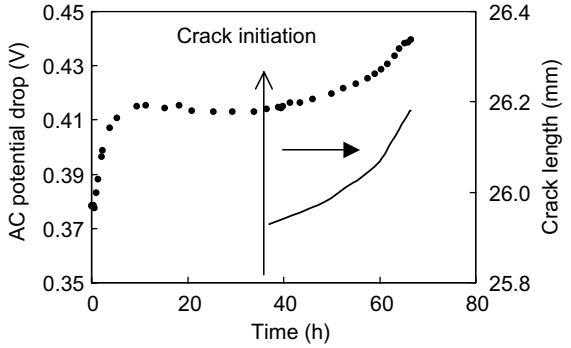

Fig. 1. The variation of ACPD (measured) and its corresponding changes in crack length as a function of time for test 1.

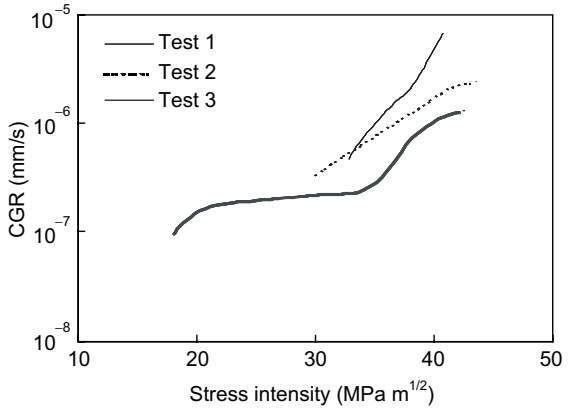

Fig. 2. Crack growth rates vs. stress intensity factor for the three SSRT tests.

stress intensity factor corresponding to the initiation of SCC were both increased with the extension rate. In addition, a three-stage curve was observed in test 3, as is characteristic of SCC.

2.3.2. Fractography of the specimens

The SCC initiated transgranularly during the tests, and then transferred to IGSCC. Extensive IGSCC was found in all three specimens. SEM observations of the crack surface adjacent to the air-fatigue pre-crack are shown in Fig. 3. A clear transition region from transgranular SCC (TGSCC) to IGSCC at the beginning stage of the crack growth can be found in the three tests. The length of TGSCC in test 1 is about one to two times of the grain size, while in test 2 the TGSCC-length is less than the grain size. In test 3, the TGSCC was more suppressed, which shows the minimum TGSCC-length among the three tests. These transition behaviors from TGSCC to IGSCC clearly show the effect of extension rate and in situ pre-cracking in test 3 on the SCC initiation.

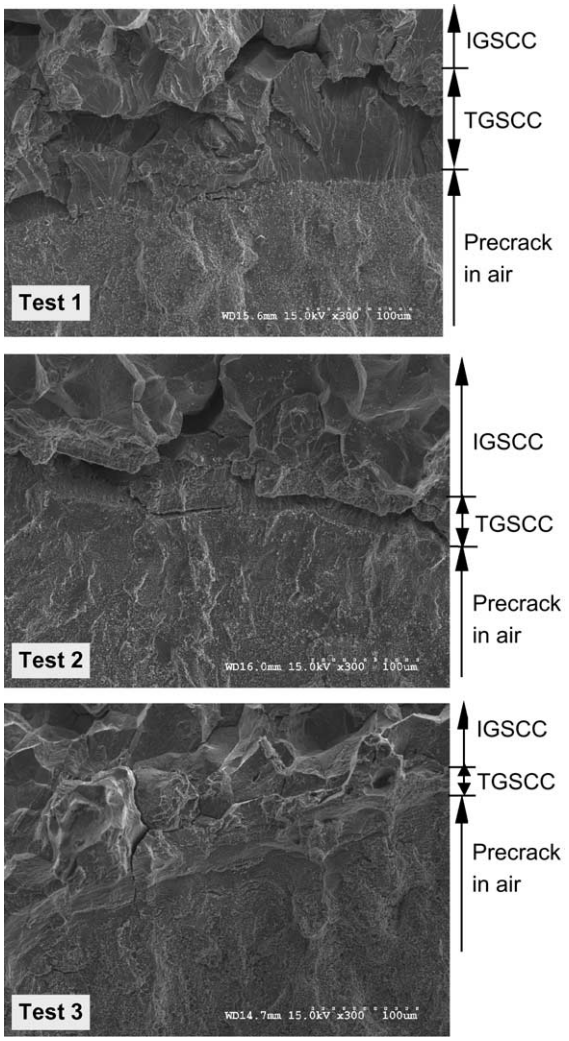

Fig. 3. SEM fractography showing the transition of SCC from transgranular to intergranular at the beginning stage of propagation. Crack growth is from bottom to top.

3. Inverse analysis to estimate the characteristic distance

The basic approach to the estimation of the characteristic distance, r_0 in Eq. (6), as stated previously, is the inverse calculation, whereby this variable is found using the test results and numerical computation. The SCC Eq. (7) calculates the change in crack length, which is then compared to the results of SSRT tests. In the process of numerical calculation, numerous solutions are obtained for the given values of indefinite variables, particularly the characteristic distance r_0 and the repassivation rate m. The optimum values of these indefinite variables are determined by minimizing the difference between the calculated and tested crack length.

The term $\dot{a}$ in Eq. (7) appears on both sides. It is assumed that the CGR on the left-hand side (LHS) is an objective function, whereas the CGR on the right-hand side (RHS) of Eq. (7) is a given function which is interpolated to the polynomial function based on test results. In the same way, the stress intensity factor, K and its rate of change, $\dot{K}$ are approximated to the polynomial functions. To solve the theoretical EAC equation, the electrode kinetic and material parameters for sensitized 304L SS listed in Table 3 are used. These are referenced from published literature, albeit with a degree of uncertainty about the repassivation kinetic parameters, such as i_0, t_0 and m [5,22]. The slip/dissolution–oxidation model [5] empirically presents the methodology for

Table 3
Standard electrode kinetic and material parameters for 304L SS

Parameter	Value
Atomic weight, M (g/mol)	55.38
Number of equivalents exchanged, z	2.67
Oxidization current density, i_0 (A/mm^2)	0.001
Fracture strain of oxide film, ε_f	0.0008
Young's modulus, E (MPa)	206 000
Dimensionless constant, β	5.46
Density, ρ (g/mm^3)	0.00786
Faraday's constant, F (C/mol)	96 500
Duration of constant i_0, t_0 (s)	0.2
Yield strength, σ_y (MPa)	196
Strain hardening exponent, n	4.1
Dimensionless constant, λ	0.11

relating m to measurable parameters, which include corrosion potential, solution conductivity, and a degree of chromium depletion along grain boundaries in terms of EPR. The range of m is given as 0.4–0.7. These values are determined based on the SSRT test conditions such as solution conductivity (0.2–0.4 μS/cm), dissolved oxygen (DO) content (>20 ppm), and 12% double-loop EPR. Since the environmental conditions are defined in detail, the acceptable range of m values is chosen. These numbers fall within the range of what might be typical from present SSRT test conditions.

For the specified range of m, and for r_0 from 1 μm to 1 mm, the differential equation was numerically solved, producing changes in the crack length as a function of time. The best-estimates of r_0 and m are determined by fitting to the measured crack length, which ensures the minimization of the root mean square (RMS) error between the calculated and measured crack lengths. The RMS error is defined as

$$\mathrm{RMS} = \sqrt{\frac{\sum_{i=1}^{N}(a_i^{\mathrm{meas}} - a_i^{\mathrm{cal}})^2}{N}}, \tag{8}$$

where N is the total number of data points and the superscripts of 'meas' and 'cal' represent 'measured' and 'calculated' crack lengths, respectively.

The calculated crack length vs. time plots, as well as measured crack length, for three cases are shown in Fig. 4. Small-scale r_0 tends to produce a reasonable fit to the test results, which is on the order of several micrometers. The values of r_0 and m, shown in Fig. 4, are the best estimates, at which the RMS values for each case are lowest for the given ranges of r_0 and m. The results indicate that the theoretical SCC equation is of use in predicting the cracking behavior when the strain rate is defined at a distance of several micrometers from a crack tip. The optimized values of m shown in Fig. 4 do not completely represent the system chemistry conditions in that these values lie within the given range of 0.4–0.7 depending on the tolerance of the RMS error. For example, the RMS error is 0.009 at best estimates of $r_0 = 2.5$ μm and $m = 0.575$ for SSRT Test 1. When the RMS error increases to 0.013, m ranges from 0.45 to 0.6, and r_0 changes from 2 to 8 μm. The small increase in RMS error, which is slightly higher than the lowest RMS one, causes m and r_0 to change significantly. However, emphasis is placed on estimating the scale of the characteristic distance.

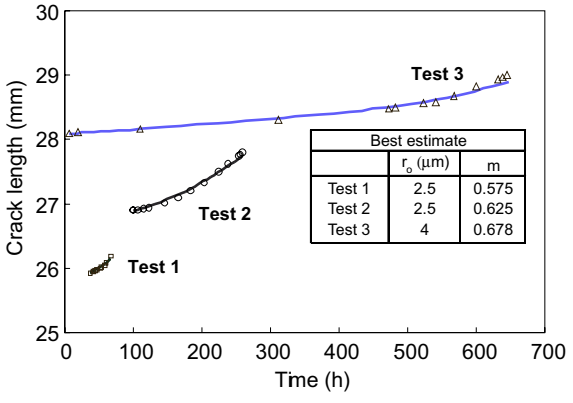

Fig. 4. Comparison of the calculated crack length (curves) and tested results (symbols), together with best estimates of the characteristic distance r_0 and the repassivation rate m for each test.

In the present study, best-estimates are used in calculating the CGR under constant load based on Eq. (7), followed by the next section. Also, it is worth discussing physical considerations concerning the characteristic distance.

4. Crack growth rate calculation under constant load

The applied load is implicitly included in the stress intensity factor. The difference in the loading mode such as the SSRT, constant load, constant displacement etc. can be expressed in terms of K and $\dot{K}$ in the SCC equations. The change in the loading mode can cause a change in the crack tip strain rate and, consequently, in the CGR. The constant load test simulates the stress/strain conditions better than the SSRT test for most reactor internals, such as the core shroud and top guide in a BWR [29].

The CGR test results performed under constant loading were collected from the published literature [30]. The outline of the test conditions is as follows. SCC tests for sensitized 304 SS were performed under constant load using CT specimens to determine the CGR in simulated BWR environments at 288 °C. The water chemistry was controlled by various combinations of hydrogen peroxide (H_2O_2), dissolved oxygen (O_2), and hydrogen (H_2). The material was furnace-sensitized and the measured double-loop EPR was 38%. The initial stress intensity factor was 31 MPa $m^{0.5}$. The details of the solution chemistry conditions and measured CGR are listed in Table 4.

In the case of a constant load, the theoretical SCC equation can be readily applied to calculate the CGR since the rate of change in the applied load is zero. When the stress intensity factor is given by $K = cP(t)f(a)$, where c is a constant, $P(t)$ is the applied load and $f(a)$ is a geometry function depending on the specimen type, it can be assumed that $\mathrm{d}P/\mathrm{d}t$ is equal to zero under constant loading. Thus, the term of $\dot{K}/K$, shown in Eq. (7), is mathematically expressed by

Table 4
Summary of CGR test results and chemistry conditions for sensitized 304 SS under constant loading

Case #	O_2 (ppb)	H_2O_2 (ppb)	H_2 (ppb)	Conductivity (μs/cm)	E_{corr} (mV_{she})	CGR (mm/s)
1	50	20	50	0.1	−90 to −80	1.2×10^{-8}
2	50	20	50	0.3	−140 to −120	2.9×10^{-8}
3	100	50	50	0.1	−50 to −40	1.3×10^{-8}
4	200	100	20	0.1	20 to 30	5.4×10^{-8}
5	200	100	20	0.3	10 to 20	6.2×10^{-8}
6	200	100	20	0.3	−60	3.2×10^{-8}
7	240	570	14	0.3	50	1.4×10^{-7}
8	440	150	50	0.1	50	1.9×10^{-7}
9	440	150	50	0.3	10	3.0×10^{-7}

All data extracted from Ref. [30].

$$\frac{\dot{K}}{K}=\frac{1}{P}\frac{\mathrm{d}P}{\mathrm{d}t}+\frac{1}{f(a)}\frac{\partial f}{\partial a}\frac{\mathrm{d}a}{\mathrm{d}t}\Rightarrow\frac{\dot{K}}{K}=\frac{1}{f(a)}\frac{\partial f}{\partial a}\frac{\mathrm{d}a}{\mathrm{d}t}. \tag{9}$$

Substitution of Eq. (9) along with the proper geometry function $f(a)$ to Eq. (7) makes the theoretical SCC equation solvable numerically. In determining the repassivation rate m, we referred to the plots given in Ref. [5], taking into account the corrosion potential and solution conductivity outlined in Table 4.

Using the theoretical SCC equation, the CGR was calculated and compared with test results. Fig. 5 shows the calculated and measured CGR, in which the calculated data are close to the measured ones as the data points are located near the diagonal dash-dotted line. In this calculation, two values of the characteristic distance are set to be 2.5 and 3.0 μm, and the applied load was manipulated to obtain the initial stress intensity factor of 31 MPa $m^{0.5}$. Depending on the choice of the characteristic distance, apparent changes in the CGR were found. For the two given values of the characteristic distance, however, the calculated results show a fair agreement with the test data. The calculated results indicate that the theoretical SCC equation is a dependable tool in predicting the CGR for stainless steels in high temperature oxygenated water. Furthermore, the strain distribution ahead of a crack tip proposed by Gao and Hwang [21] can be used to define the crack tip strain rate which is an essential parameter to determine the loading condition in the slip/dissolution–oxidation model. In addition, the calculation supports the fact that the characteristic distance should be defined on the order of several micrometers ahead of a crack tip. This is consistent with the experimental measurements of crack tip strain which showed that, despite the small strain theory assumptions used in obtaining crack tip strain expressions, the continuum mechanics solutions predict reasonably the near-surface crack tip strains that were only a few micrometers away from the crack tip surface [18].

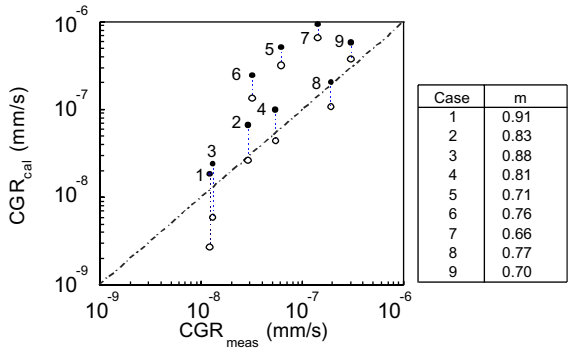

Case	m
1	0.91
2	0.83
3	0.88
4	0.81
5	0.71
6	0.76
7	0.66
8	0.77
9	0.70

Fig. 5. Comparison between measured (Table 4) and calculated crack growth rate with two values of the characteristic distance (2.5 and 3 μm). The repassivation rate of m for each case is listed in the table. Dashed lines between the solid and open circles represent the same case with different r_0, and the diagonal dash-dotted line is provided as a guide to the eye.

Calculated results produced from three cases of 5–7 show relatively large differences from the test data. According to the slip/dissolution–oxidation model, a lower value of m results from such conditions as higher corrosion potential, solution conductivity and degree of sensitization. These three cases correspond to the condition of having a lower value of m. Since the repassivation rate m is determined by the bulk water chemistry, it is probable that the m values used in the calculation do not completely characterize the crack tip chemistry conditions. The difference in water chemistry between bulk and crack tip environments can cause difficulties in determining m.

5. Discussion

5.1. Dependency of the characteristic distance on the cracking mode

The correct choice of the characteristic distance for the CGR estimation is vital if acceptable results are to be

Table 5
Summary of CGR test results produced by VTT Manufacturing Technology

Load line displacement rate (mm/s)	Stress intensity (MPa $m^{0.5}$)	$\dot{K}$ (MPa $m^{0.5}$/s)	CGR (mm/s)	Percentage of IG cracking
1×10^{-6}	21.1	2.92×10^{-5}	1.1×10^{-6}	0
5×10^{-7}	26.9	6.94×10^{-6}	5.9×10^{-7}	5
2.1×10^{-7}	28.9	4.41×10^{-6}	4.5×10^{-7}	70
2×10^{-6}	31.2	3.85×10^{-5}	2.2×10^{-6}	0

All data extracted from Ref. [31] except $\dot{K}$, estimated from test data.

obtained. As outlined in the previous section, the appropriate range of the characteristic distance is on the order of several micrometers. However, the calculated CGR is very sensitive to small changes in the characteristic distance. In this section, we discuss a potential factor, which may affect the variation of the characteristic distance using the experimental data produced by VTT Manufacturing Technology [31].

Tests were performed under rising/constant displacement type loading, using three-point-bending (3PB) geometry specimens ($10\times10\times55$ mm, Charpy size) which were made of AISI 304 stainless steel in mill-annealed + sensitized (620 °C/24 h) conditions. Load line displacement rate intentionally varied during each test in order to reduce the number of tests needed to determine the influence of the loading rate on CGR. Tests were carried out in simulated BWR water with conductivity of 0.2 μS/cm at outlet, DO levels of 300 ppb and corrosion potential of 200 mV_{she}. Changes in crack length, load, loading rate, stress intensity factor, and J-integral values were well-arranged and plotted in Ref. [31]. Based on given data, the rate of change in the stress intensity factor was manually calculated. The estimation of $\dot{K}$ includes unavoidable errors due to the fact that the applied load behaves in a jagged way and it is impossible to read those values exactly with the naked eyes. Important data for the following analysis are summarized in Table 5. It should be noted that all the test results shown in Table 5 are the average values for each loading step. It is assumed that constant load is applied at the specific load line displacement rate in calculating $\dot{K}$.

The CGR was calculated using Eq. (7) and compared with the test results listed in Table 5. The appropriate value of m is close to 0.6, which was determined from Ref. [5]. In order to investigate the effect of the characteristic distance on cracking behavior, three values of r_0, 3, 7, and 10 μm, were used. Fig. 6 shows a comparison between the measured and calculated CGR for the three cases of the characteristic distance. It can be seen that there is not much difference in the calculated CGR for the specified value of the characteristic distance while a small variation of the characteristic distance brings about significant changes in the CGR. This is because the term $(1/r_0)$ predominates over $(2\dot{K}/K)$ shown in

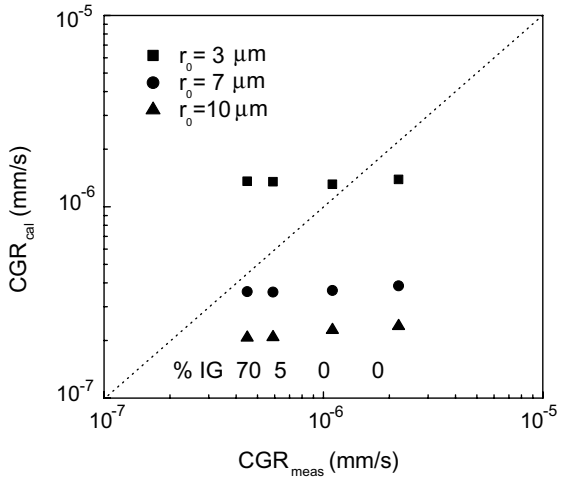

Fig. 6. Comparison between measured and calculated CGR as a function of characteristic distance. All data – measured CGR and % IG cracking, were obtained from Ref. [31]. The diagonal dashed line is provided as a guide to the eye.

Eq. (6). One thing to be noticed about this calculation is that it is likely that there is a correlation between the characteristic distance and the % IG cracking. The calculated CGR corresponds well with the measured CGR at a small characteristic distance (3 μm) when transgranular cracking is dominant. At a relatively large characteristic distance (7 μm), both results show a good agreement in the higher % IG cracking region. The dependency of the characteristic distance on the cracking mode might account for the determination of the accurate size of the characteristic distance.

5.2. Physical significance of the characteristic distance

It is worth discussing the physical significance of the characteristic distance in the cracking event. It has been suggested that, due to the environmentally assisted cleavage mechanism [7], the crack in the oxide film can proceed for a significant distance into a ductile matrix before coming to a stop. The assumptions about this

suggestion are: the interface between the film and the matrix is coherent, or the film is strongly bonded to the matrix. Estimates of the extent of the crack arrest distance into a matrix were made by applying the law of energy conservation in conjunction with a microscopic crack arrest condition for face-centered cubic materials [32]. The extent of crack jump distances is on the order of 1–10 μm. The characteristic distance derived in this study lies in this range. However, there is no clear evidence that the crack jump distance is related to the characteristic distance in this study except that it is of comparable magnitude.

Another explanation for the characteristic distance is as follows. Basically, the strain rate should be defined at the very tip of a crack. However, strain approaches infinity as the distance goes to zero. It is assumed that a certain region exists ahead of a crack tip within which strain has the same value. Hence, the crack tip strain rate may be represented by a certain value at a crack over the characteristic distance.

6. Conclusion

1. The theoretical SCC equations have been implemented in estimating the CGR in austenitic stainless steels in high-temperature oxygenated water.
2. The characteristic distance, one of the unknown variables included in the equation, was determined quantitatively by SSRT test results and numerical calculations. The size is on the order of several micrometers.
3. The CGR under constant load was calculated by using the theoretical SCC equation and the determined characteristic distance. The comparison of calculation with experimental CGR shows a fair agreement in relatively high quality water environments, indicating the applicability of the theoretical SCC equations for quantification of CTSR and CGR of stainless steel in high temperature oxygenated water.
4. It is probable that the size of the characteristic distance is related to the cracking mode. When IG cracking is dominant, the relatively higher value of the characteristic distance presents reliable results.

Acknowledgements

This research was supported by the Ministry of Education, Sports, Culture, Science and Technology under the grant-in-aid for COE Research (No. 11CE2003). The authors wish to thank F.P. Ford for fruitful discussions during this study and S. Ishikawa for the cooperation in performing the tests.

References

[1] R.M. Horn, G.M. Gordon, F.P. Ford, et al., Nucl. Eng. Des. 174 (1997) 313.
[2] A. Turnbull, Corros. Sci. 34 (1993) 921.
[3] P.L. Andresen, F.P. Ford, Int. J. Pres. Ves. Pip. 59 (1994) 61.
[4] P.L. Andresen, F.P. Ford, S.M. Murphy, et al., in: Daniel Cubcciotti (Ed.), Proceedings of the 4th International Symposium on Environmental Degradation of Materials in Nuclear Power Systems – Water Reactors, NACE, 1990, p. 1.
[5] F.P. Ford, P.L. Andresen, in: S.M. Bruemmer (Ed.), Parkins Symposium on Fundamental Aspects of Stress Corrosion Cracking: Proceedings of a Symposium Sponsored by TMS-ASM-MSD Corrosion and Environmental Effects Committee, TMS, 1992, p. 43.
[6] P.L. Andresen, F.P. Ford, Mater. Sci. Eng. A 103 (1988) 167.
[7] F.P. Ford, D.F. Taylor, P.L. Andreson, et al., in: EPRI final report RP2006-6, Electric Power Research Institute, 1987.
[8] J. Congleton, T. Shoji, R.N. Parkins, Corros. Sci. 25 (1985) 633.
[9] D.P.G. Lidbury, in: R.P. Gangloff (Ed.), Proceedings of an International Symposium on Embrittlement by Localized Crack Environment, AIME, 1984, p. 149.
[10] G. Gabetta, K. Torronen, in: W.H. Cullen (Ed.), Proceedings of the Second International Atomic Energy Agency Specialists Meeting on Subcritical Crack Growth, Materials Engineering Associates, 1986, p. 131.
[11] R.N. Parkins, G.P. Marsh, J.T. Evans, in: H. Okada, R. Staehle (Eds.), Predictive methods for assessing corrosion damage to BWR piping and PWR steam generators, NACE, 1982, p. 249.
[12] B.P. Somerday, L.M. Young, R.P. Gangloff, Fatigue Fract. Eng. Mater. Struct. 23 (2000) 39.
[13] Lisa M. Young, Peter L. Andresen, Thomas M. Angeliu, in: Proceedings of Corrosion 2001, NACE International, 2001, Paper 01131.
[14] P.L. Andresen, in: G.J. Theus, J.R. Weeks (Eds.), Proceedings of the 3rd International Symposium on Environmental Degradation of Materials in Nuclear Power Systems – Water Reactors, The Metallurgical Society, 1988, p. 301.
[15] J.R. Rice, W.J. Drugan, T.-L. Sham, ASTM STP 700, ASTM, 1980, p. 189.
[16] R.A. Mayville, T.J. Warren, P.D. Hilton, Trans. ASME 109 (1987) 188.
[17] E.D. Eason, E.E. Nelson, J.D. Gilman, in: Proceedings of the ASME PVP Conference, Changing priorities of codes and standards, ASME, 1994, p. 131.
[18] W.W. Gerberich, D.L. Davidson, M. Kaczorowski, J. Mech. Phys. Solids 38 (1990) 87.
[19] S.J. Hudak Jr., D.L. Davidson, R.A. Page, in: R.P. Gangloff (Ed.), Proceedings of an International Symposium on Embrittlement by Localized Crack Environment, AIME, 1984, p. 173.
[20] D.R. Williams, D.L. Davidson, J. Lankford, Exp. Mech. 20 (1980) 134.

[21] Y.C. Gao, K.C. Hwang, in: D. Francois (Ed.), Proceedings of the 5th International Conference on Fracture, Pergamon, 1982, p. 669.
[22] T. Shoji, S. Suzuki, R.G. Ballinger, in: Proceedings of the 7th International Symposium on Environmental Degradation of Materials in Nuclear Power Systems-Water Reactors, NACE, 1995, p. 881.
[23] S. Suzuki, T. Shoji, Y.-S. Yi, et al., in: Proceedings of the 8th International Symposium on Environmental Degradation of Materials in Nuclear Power Systems-Water Reactors, ANS, 1997, p. 695.
[24] T.M. Angeliu, in: Proceedings of Corrosion 2000, NACE International, 2000, Paper 185.
[25] M.J. Anciaux, Metall. Trans. 12A (1981) 1981.
[26] Japan Industrial Standard G 0580, Japan, JIS, 1986.
[27] P. Lidar, I.S. Hwang, R.G. Ballinger, in: Proceedings of the 5th International Symposium on Environmental Degradation of Materials in Nuclear Power Systems-Water Reactors, ANS, 1991, p. 126.
[28] ASTM E399-90, Annual book of ASTM standards, ASTM, 1990, p. 412.
[29] A.J. Jacobs, G.P. Wozadlo, S.A. Wilson, Corrosion 49 (1993) 145.
[30] E. Kikuchi, M. Itow, J. Kuniya, et al., Corrosion 53 (1997) 306.
[31] A. Toivonen, P. Aaltonen, ICG/EAC Meeting, Williamsburg, VA, 2000.
[32] K. Sieradzki, R.C. Newman, Philos. Mag. A 51 (1985) 95.